First-Principles Approach to Model Electrochemical Reactions: Understanding the Fundamental Mechanisms behind Mg Corrosion

Sudarsan Surendralal,[1] Mira Todorova,[1,*] Michael W. Finnis,[2] and Jörg Neugebauer[1]
[1]*Department of Computational Materials Design, Max-Planck-Insitut für Eisenforschung GmbH, Max-Planck-Strasse 1, D-40237 Düsseldorf, Germany*
[2]*The Thomas Young Centre, Department of Materials and Department of Physics, Imperial College London, London SW7 2AZ, United Kingdom*

(Received 23 February 2018; published 12 June 2018)

Combining concepts of semiconductor physics and corrosion science, we develop a novel approach that allows us to perform *ab initio* calculations under controlled potentiostat conditions for electrochemical systems. The proposed approach can be straightforwardly applied in standard density functional theory codes. To demonstrate the performance and the opportunities opened by this approach, we study the chemical reactions that take place during initial corrosion at the water-Mg interface under anodic polarization. Based on this insight, we derive an atomistic model that explains the origin of the anodic hydrogen evolution.

DOI: 10.1103/PhysRevLett.120.246801

Many of the technological challenges we presently face, such as improving battery materials, electrocatalysis, fuel cells, or corrosion protection, originate from reactions at solid-liquid electrochemical interfaces. To address and eventually overcome these challenges requires accurate modeling techniques. First-principles calculations, which are free from fitting parameters, would be the method of choice. In recent years, several approaches have been developed to address the issue of constant electrode potential [1–8], a prerequisite to study electrochemical reactions. These approaches are thermodynamically open with respect to electrons, but canonical with respect to protons, as pointed out by Rossmeisl and co-workers [9]. For example, enforcing a specific *p*H value would require an exchange of protons with a chemical reservoir. Such a grand-canonical exchange is not compatible with the presently available *ab initio* molecular dynamics schemes. A successful strategy to partly overcome this issue is to start with a given atomic structure at the interface and compute the resulting electrode potential and energy using standard *ab initio* molecular dynamics approaches [10]. A large number of electrochemical studies have been carried out successfully using this approach [10–12]. A restriction of this approach is that it is limited to equilibrium configurations at the interface. Thus, a method for performing *ab initio* molecular dynamics simulations that are grand canonical in both electrons and atoms or protons is still lacking.

The fundamental requirement for a grand-canonical description and the difficulties with its realization within a standard density functional theory (DFT) code with periodic boundary conditions can be illustrated using the example of two electrodes in an electrolytic cell (cf. Fig. 1).

To ensure a constant electrode potential U, electrons have to be transferred from the anode (positively charged electrode) to the cathode (negatively charged electrode). The resulting electric field drives negatively charged ions such as OH^- to the positively charged anode and positively charged cations such as H^+ (protons) to the negatively charged cathode. A consistent description of this fundamental mechanism thus requires that each electrode is thermodynamically open to both electrons and protons. However, while a single electrode is intrinsically grand canonical, the full electrolytic cell, which contains both the

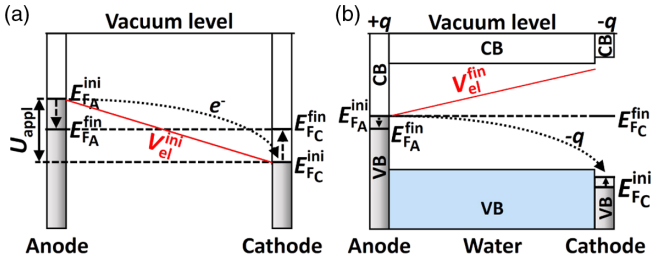

FIG. 1. Schematic representation of the concept used to realize an electrolytic cell. (a) Alignment between two metal electrodes before (superscript "ini") and after (superscript "fin") charge transfer. The charge transfer leads to equal Fermi energies E_F and zero bias and thus prevents the realization of an electric field. The red line shows the electrostatic potential before the charge transfer. (b) A doped semiconductor electrode allows us to control the position of the Fermi level. The type (here, p type) and concentration of dopants controls the polarity and magnitude of the field. The red line shows the electrostatic potential realized by the charge transfer. The slope of the potential is proportional to the induced electric field.

positively and negatively charged electrode, is canonical for both electrons and protons.

If we were able to utilize this canonical setup, where the number of electrons and protons remains constant throughout the simulation, it would be possible to circumvent the previously mentioned difficulty and describe electrochemical systems under realistic conditions. Unfortunately, trying to realize such a cell in a conventional DFT code with periodic boundary conditions will fail for the following reason. In order to realize a potentiostat and thus an electric field between the two electrodes, the Fermi level of the two electrodes has to be different [see cathode and anode Fermi level marked in Fig. 1(a)]. In standard DFT supercell calculations, however, a mandatory condition is that the Fermi level is constant throughout the cell, which kills any field between the two electrodes [Fig. 1(a)]. A solution to address this issue has been proposed by Otani and Sugino [4], but requires major modifications to a standard DFT code since it is based on a modified Poisson solver using Green's function techniques.

To overcome this fundamental limitation, we propose a novel type of computational electrode. Rather than using two metal electrodes, we replace one electrode by a doped semiconductor [Fig. 1(b)]. To understand the mechanism, let us first consider the case where the semiconductor is not doped. For this case, and if the Fermi level of the metal electrode falls within the band gap of the semiconductor electrode, the two electrodes are decoupled and no charge transfer from one to the other electrode occurs. To build up a potential difference (potentiostat) between the two electrodes, charge needs to be transferred from one electrode to the other. We therefore dope the semiconductor electrode p type (to charge it negatively and make it the cathode) or n type (to charge it positively and make it the anode). Figure 1(b) shows that, in the first case, electrons are transferred from the Fermi level of the metal to the p-doped electrode, leaving the metal electrode with a positive charge q and the semiconducting electrode with a negative charge $-q$. Because of Gauss law, this charge transfer induces a potential bias U as well as an electric field. Controlling the doping charge q enables us to control the bias and field. To change the polarity of the field, the p-type electrode is replaced by a n-type one.

Identifying a suitable semiconducting electrode material that allows us to realize these concepts in a realistic electrochemical setup turned out to be not straightforward. Ideally, to allow maximum control, the band gap of the electrode should be larger than that of water and it would be aligned such that its conduction band (CB) minimum (valence band maximum) is above (below) the one of water [see Fig. 1(b)]. To construct such an electrode, we experimented first with conventional wide band gap semiconductor materials. Our computational studies using materials such as AlN ($E_{\mathrm{gap}} = 6.02$ eV [13]) or MgO ($E_{\mathrm{gap}} = 7.77$ eV [14]) showed, however, two severe shortcomings. First, the actual DFT–Perdew-Burke-Ernzerhof (PBE) [15] band gap for these materials is about ~4.20 eV (AlN) and ~4.53 eV (MgO), implying a rather limited variability of the potential and thus the electric field. Second, the periodicity of the supercell requires that the two electrodes are commensurable; i.e., their lateral lattice constant cannot be chosen freely. Because of the large deformation potentials of these materials, a significant further reduction of the band gap occurred (it became smaller than 2.5 eV).

These limitations of conventional semiconductors led us to extend the search to unconventional insulators, identifying Ne ($E_{\mathrm{gap}} = 21.6$ eV) as the crystal with the largest band gap known in nature [16]. Even though our computed DFT-PBE band gap for Ne is significantly smaller ($E_{\mathrm{gap}} = 11.48$ eV), it nevertheless fulfills the requirement. Ne turned out to be an excellent computational electrode material also with respect to other properties: since the only interaction between the Ne atoms is van der Walls bonding, its deformation potential is almost negligible. In addition, Ne is chemically inert so that chemisorption or alloy formation on this electrode is suppressed. We also find that even a single Ne layer prevents permeation of water molecules or of its residues, such as H^+ or OH^-.

To dope the Ne electrode, we do not use explicit dopants, since this would only allow us to change the electrode charge by integer numbers. Rather, we use the concept of pseudoatoms with fractional proton numbers [17]. To construct a Ne electrode consisting of n_{Ne} atoms with charge q, we change the proton number of Ne from Z_{Ne} to $Z_{\mathrm{Ne}} + q/n_{\mathrm{Ne}}$. To ensure that the pseudoatom is charge neutral, the number of valence electrons is also increased by q/n_{Ne}. Since q/n_{Ne} is a small fraction of an electron, the band structure (band gap) of the Ne electrode remains almost unchanged except that it contains q excess electrons in the conduction or (for negative q values) q holes in the valence band. This construction gives us full control over the electrode charge and thus provides a central element to construct a static or dynamic potentiostat, i.e., with a constant or variable applied bias.

With the concept of the doped Ne electrode, the setup of an electrolytic electrochemical cell employing standard DFT supercell calculations is straightforward. Here we use the Vienna *ab initio* simulation package (VASP) [18,19] with generalized gradient approximation–PBE [15] as the exchange-correlation functional (see Supplemental Material [20]). The space between the metal and the Ne electrode is filled with an electrolyte (here 64 explicit H_2O molecules), while a vacuum region is added on the outside of the electrodes. Since the potential between the two electrodes is U, we include a dipole correction in the middle of the vacuum region [27]. This allows the potential drop across the cell while restoring the overall periodic spatial variation of the potential [28].

The above approach enables us to obtain experimental observables and to conveniently control the experimentally

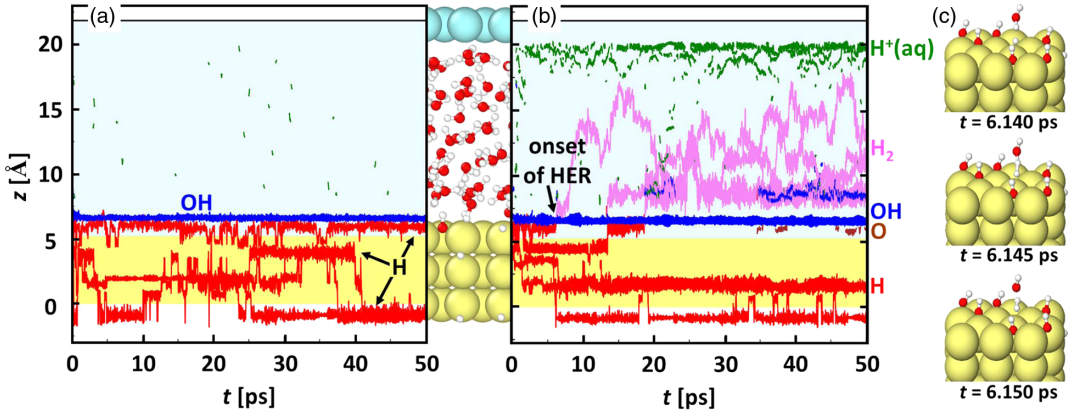

FIG. 2. *Ab initio* computed trajectories of the atomic and molecular species formed when Mg is exposed to water for (a) open circuit conditions and (b) applying a linear increasing voltage (see text). Trajectories are shown in a projection along the normal to the Mg surface. Blue, red, violet, green, and brown lines mark OH, H, H_2, H^+ (aq.), and O, respectively. The onset of the H_2 evolution reaction is indicated in (b) by a black arrow. To focus on the relevant reaction products Mg-water trajectories are shown as yellow (blue) colored background. The atomic geometry of the electrolytic cell is visualized in the figure between (a) and (b). Atoms are shown as colored spheres: Mg (yellow), Ne (turquoise), oxygen (red), hydrogen (gray). (c) Snapshots of the HER extracted from the MD trajectory of the system under applied bias potential.

accessible parameters. For example, the voltage obtained by the dipole correction [27] is a direct measure of the electrode potential at the interface. The total dipole moment μ_{tot} of the system, which is computed from the dipole correction, varies with the amount of charge transfer between the electrodes and reflects the extent to which the aqueous (aq.) electrolyte screens the applied electric field. Consequently, control of μ_{tot} during the course of the simulation controls the electrode potential of the interface. This allows us to adjust the charge supplied to the system to maintain a constant potential dynamically, in analogy to an experimental static potentiostat.

The control cycle works as follows. In a first step, the applied potential bias separates cations and anions. Positively (negatively) charged ions such as H^+/OH^- migrate towards the negatively (positively) charged cathode (anode) thus counteracting the applied field. Bringing these charged particles to the electrode changes the electrode-electrolyte interface dipoles and reduces the applied bias U by ΔU. To keep the applied potential constant, additional charge is added to the electrode, in analogy to what is done in experiment. Note that by using charge neutral doped Ne atoms to add the charge [29], the total system remains charge neutral; i.e., it is free of an artificial compensating background and thus does not need any corrections. By this feedback loop, we have effectively created a static potentiostat and are furthermore able to directly measure the Faradaic current passing through the electrochemical system.

To evaluate the applicability and performance of the proposed approach, we consider Mg corrosion under anodic conditions. The reason for this selection is that Mg is a technologically highly attractive material for achieving lightweight engineering solutions (e.g., to increase fuel efficiency in aerospace or automobile applications), for biodegradable materials and for battery electrodes [30–32]. It exhibits, however, also a number of technological issues such as a high vulnerability to wet corrosion. A particularly puzzling and technologically highly detrimental phenomenon of Mg corrosion occurs under anodic polarization, where extremely high corrosion rates together with H_2 evolution are observed [33,34]. According to the fundamental corrosion concepts, H_2 evolution should only occur at the negatively charged cathode, e.g., via the reaction $2H^+ + 2e^- \rightarrow H_2$. This counterintuitive behavior has been known for 150 years [33] and is called anodic hydrogen evolution [31] or negative difference effect. It has been intensively studied both experimentally [35–40] and theoretically [41,42]. However, a consensus about the atomistic mechanism or reactions has not been reached so far. The approach developed and described here allows a fully *ab initio* description of the chemical reactions that occur when Mg is anodically polarized and brought into contact with water.

We first consider the case without an electric field (open circuit conditions). Figure 2(a) shows the trajectories along the interface normal (z axis). To highlight the chemical reactions, only the trajectories of the various ions are shown, while the trajectories of the water molecules and the Mg atoms are blended out. We find that water molecules spontaneously dissociate at the Mg surface. The OH groups occupy the hollow adsorption sites, in agreement with results of previous *ab initio* molecular-static simulations with implicit water [41], and reach a 1/3 monolayer coverage. In contrast to the OH groups that once adsorbed remain on this site, the adsorbed H atoms are highly mobile and easily penetrate the electrode: as can be

seen in Fig. 2, they jump between the Mg sublayers and the surface on a timescale of a few picoseconds.

To study the initiation of Mg corrosion under anodic polarization, we repeat the molecular dynamics (MD) simulations with the electric field switched on. The potential is controlled in the manner of a linear sweep voltammetry experiment. We start at an initial applied voltage of 0.86 V and raise it every 5 ps by 0.17 V. Because of the high chemical reactivity of the Mg electrode, even in the short time of 50 ps, a surprisingly large number of reactions takes place. One reaction observed once again is the dissociation of water molecules at the initially pure Mg surface into H^+ and OH^- ions. However, in contrast to the open circuit case, the OH coverage does not stop at 1/3 monolayer, but increases with time until a full monolayer is reached. The resulting OH monolayer is stable at anodic potentials, consistent with previous *ab initio* studies using static calculations and an implicit solvent model for water [41].

While the above reaction is canonical—the number of H and O atoms at the anode remains constant—we also find reactions where the species number changes. These are related to a field induced dissociation of H_2O, with H^+ (aq.) migrating to the Ne cathode while OH^- remains on the Mg anode, as seen from the trajectories in Fig. 2(b). The field driven transfer of the protons to the Ne electrode happens through a Zundel-to-Zundel Grotthuss-type hopping mechanism reported in previous Car-Parinello *ab initio* simulations of bulk water [43,44] and experiments [45]. The proton transport can also be inferred from the steep increase in charge during the same time range, as seen in Fig. 3: the transport of the proton to the Ne electrode screens the applied electric field, resulting in a drop in the voltage and therefore more positive charge needs to be pumped into the Mg electrode to maintain a constant applied voltage.

As also revealed by Fig. 2(b), the hydrogen evolution reactions (HERs) takes place under anodic conditions but not under open circuit conditions [Fig. 2(a)]. As discussed above, this "negative difference effect" at anodically

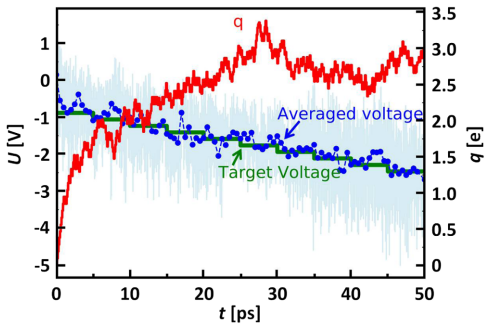

FIG. 3. Evolution of the voltage and the charge (red) during the MD run. The instantaneous voltage is shown in light blue, its averaged value in blue and the targeted voltage in green.

polarized Mg interfaces has been observed by many experimental studies, but as mentioned before, its origin is highly debated. The occurrence of the HER only at higher OH coverages agrees with experimental observations and has been interpreted by suggesting that increasing OH coverage catalyzes the HER [39,42].

Our *ab initio* setup allows us to inspect the reaction at the atomic level and to identify its underlying atomistic mechanism. Figure 2(c) shows snapshots of the reaction, extracted from the *ab initio* molecular dynamics trajectories. As can be seen, a water molecule binds to a H atom adsorbed on the Mg surface, dissociates and leaves a H_2 molecule and an OH^- ion. At a first glance, this looks like a "conventional" Heyrovsky reaction in an alkaline medium: $H_{ad} + H_2O + e^- \rightarrow H_2 + OH^-$. However, since this reaction requires excess electrons, it has been assumed that it can occur only at the cathode. At an anode, where electrons are deficient, such a reaction has never been considered.

To understand why this reaction occurs despite contradicting present concepts in electrochemistry, we analyzed the reaction in detail. Inspecting the local density of states and differences in the charge density, we find that the adsorbed H is not charge neutral, but a singly negative H^-, even under the condition of a positively charged Mg surface. The reason is the high polarizability of the Mg valence electrons, which gives rise to a large spill-out region of its electrons, causing unusual adsorption phenomena [46]. The reaction can thus be described as $H^-_{ad} + H_2O \rightarrow H_2 + OH^-$; i.e., the excess electron is provided by the adsorbed H itself rather than by the anode. In the absence of a potential (open circuit conditions), the reaction does not occur [see Fig. 2(a)], because the attractive electrostatic interaction between the OH^- ion and the anode, which is critical to make this reaction exothermic, is absent.

In conclusion, by making extensive use of semiconductor concepts and methodology, we designed an approach that allows performing *ab initio* simulations under controlled potentiostat conditions for electrochemical systems. The proposed concept of a computational electrode comprising a variably doped Ne electrode can be straightforwardly implemented in existing DFT codes and opens the opportunity to study electrochemical reactions under controlled conditions of applied voltage and electric current that are directly related to experiment. Comparing the potentials applied using the presented method to the experimentally measured ones requires the capability to align the calculated potentials on an absolute scale (i.e., with respect to the vacuum level or the standard hydrogen electrode). This will allow us to directly discuss, for example, overpotentials of reactions or (dynamic) Pourbaix diagrams. Applying the concept to one of the most controversially discussed corrosion topics of the recent decades—the origin and role of hydrogen evolution at anodically polarized Mg—showed the capability of the

approach to study and discover mechanisms and reactions that were hitherto inaccessible to first-principles simulation.

Funding by the IMPRS-SurMat is gratefully acknowledged. This work is supported by the Cluster of Excellence RESOLV (EXC 1069) funded by the Deutsche Forschungsgemeinschaft. M. W. F. acknowledges the support from EPSRC under the program Grant No. HEmS EP/L014742/1.

*Corresponding author.
m.todorova@mpie.de

[1] A. Y. Lozovoi, A. Alavi, J. Kohanoff, and R. M. Lynden-Bell, J. Chem. Phys. **115**, 1661 (2001).
[2] J. K. Nørskov, J. Rossmeisl, A. Logadottir, L. Lindqvist, J. R. Kitchin, T. Bligaard, and H. Jónsson, J. Phys. Chem. B **108**, 17886 (2004).
[3] E. Skúlason, G. S. Karlberg, J. Rossmeisl, T. Bligaard, J. Greeley, H. Jónsson, and J. K. Nørskov, Phys. Chem. Phys. **9**, 3241 (2007).
[4] M. Otani and O. Sugino, Phys. Rev. B **73**, 115407 (2006).
[5] N. Bonnet, T. Morishita, O. Sugino, and M. Otani, Phys. Rev. Lett. **109**, 266101 (2012).
[6] J.-S. Filhol and M. Neurock, Angew. Chem., Int. Ed. Engl. **45**, 402 (2006).
[7] C. D. Taylor, S. A. Wasileski, J.-S. Filhol, and M. Neurock, Phys. Rev. B **73**, 165402 (2006).
[8] J. Cheng and M. Sprik, Phys. Chem. Phys. **14**, 11245 (2012).
[9] M. Nielsen, M. E. Björketun, M. H. Hansen, and J. Rossmeisl, Surf. Sci. **631**, 2 (2015).
[10] J. Rossmeisl, E. Skúlason, M. E. Björketun, V. Tripkovic, and J. K. Nørskov, Chem. Phys. Lett. **466**, 68 (2008).
[11] E. Skúlason, V. Tripkovic, M. E. Björketun, S. Gudmundsdóttir, G. Karlberg, J. Rossmeisl, T. Bligaard, H. Jónsson, and J. K. Nørskov, J. Phys. Chem. C **114**, 18182 (2010).
[12] S. Schnur and A. Groß, New J. Phys. **11**, 125003 (2009).
[13] M. Feneberg, R. A. R. Leute, B. Neuschl, K. Thonke, and M. Bickermann, Phys. Rev. B **82**, 075208 (2010).
[14] D. M. Roessler and W. C. Walker, Phys. Rev. **159**, 733 (1967).
[15] J. P. Perdew, K. Burke, and M. Ernzerhof, Phys. Rev. Lett. **77**, 3865 (1996).
[16] M. Fox, *Optical Properties of Solids* (Oxford University Press, New York, 2010), Vol. 3.
[17] K. Shiraishi, J. Phys. Soc. Jpn. **59**, 3455 (1990).
[18] G. Kresse and J. Hafner, Phys. Rev. B **47**, 558 (1993).
[19] G. Kresse and J. Furthmüller, Phys. Rev. B **54**, 11169 (1996).
[20] See Supplemental Material at http://link.aps.org/supplemental/10.1103/PhysRevLett.120.246801 for additional details, which includes Refs. [21–26].
[21] P. E. Blöchl, Phys. Rev. B **50**, 17953 (1994).
[22] G. Kresse and D. Joubert, Phys. Rev. B **59**, 1758 (1999).
[23] W. L. Jorgensen, J. Chandrasekhar, J. D. Madura, R. W. Impey, and M. L. Klein, J. Chem. Phys. **79**, 926 (1983).
[24] S. Plimpton, J. Comput. Phys. **117**, 1 (1995).
[25] A. Kohlmeyer, C. Hartnig, and E. Spohr, J. Mol. Liq. **78**, 233 (1998).
[26] E. Spohr, J. Phys. Chem. **93**, 6171 (1989).
[27] J. Neugebauer and M. Scheffler, Phys. Rev. B **46**, 16067 (1992).
[28] See Fig. 1 in the Supplemental Material.
[29] The core and valence charge are changed by modifying the corresponding parameters in the pseudopotential file: in VASP, this is the ZVAL tag in the Ne POTCAR file.
[30] T. B. Abbott, Corrosion **71**, 120 (2014).
[31] M. Esmaily, J. E. Svensson, S. Fajardo, N. Birbilis, G. S. Frankel, S. Virtanen, R. Arrabal, S. Thomas, and L. G. Johansson, Prog. Mater. Sci. **89**, 92 (2017).
[32] R. Van Noorden, Nature (London) **507**, 26 (2014).
[33] W. Beetz, London, Edinburgh, and Dublin Philos. Mag. J. Sci. **32**, 269 (1866).
[34] R. Glicksman, J. Electrochem. Soc. **106**, 83 (1959).
[35] N. Birbilis, A. D. King, S. Thomas, G. S. Frankel, and J. R. Scully, Electrochim. Acta **132**, 277 (2014).
[36] M. Curioni, Electrochim. Acta **120**, 284 (2014).
[37] M. Taheri, J. R. Kish, N. Birbilis, M. Danaie, E. A. McNally, and J. R. McDermid, Electrochim. Acta **116**, 396 (2014).
[38] G. Williams, N. Birbilis, and H. N. McMurray, Electrochem. Comm. **36**, 1 (2013).
[39] S. H. Salleh, S. Thomas, J. A. Yuwono, K. Venkatesan, and N. Birbilis, Electrochim. Acta **161**, 144 (2015).
[40] G. S. Frankel, A. Samaniego, and N. Birbilis, Corros. Sci. **70**, 104 (2013).
[41] K. S. Williams, J. P. Labukas, V. Rodriguez-Santiago, and J. W. Andzelm, Corrosion **71**, 209 (2015).
[42] J. A. Yuwono, N. Birbilis, K. S. Williams, and N. V. Medhekar, J. Phys. Chem. C **120**, 26922 (2016).
[43] P. L. Geissler, C. Dellago, D. Chandler, J. Hutter, and M. Parrinello, Science **291**, 2121 (2001).
[44] A. M. Saitta, F. Saija, and P. V. Giaquinta, Phys. Rev. Lett. **108**, 207801 (2012).
[45] S. T. Roberts, P. B. Petersen, K. Ramasesha, A. Tokmakoff, I. S. Ufimtsev, and T. J. Martinez, Proc. Natl. Acad. Sci. U.S.A. **106**, 15154 (2009).
[46] S.-T. Cheng, M. Todorova, C. Freysoldt, and J. Neugebauer, Phys. Rev. Lett. **113**, 136102 (2014).